ARTICLE
Journal of Cellular Biochemistry 115:1594–1608 (2014)

Journal of Cellular Biochemistry

Novel Target Genes of RUNX2 Transcription Factor and 1,25-Dihydroxyvitamin D3

Alexandre S. Stephens* and Nigel A. Morrison

School of Medical Science, Griffith University Gold Coast Campus, Southport, Queensland 4215, Australia

ABSTRACT

The RUNX2 transcription factor is indispensable for skeletal development and controls bone formation by acting as a signaling hub and transcriptional regulator to coordinate target gene expression. A signaling partner of RUNX2 is the nuclear vitamin D receptor (VDR) that becomes active when bound by its ligand 1,25-dihydroxyvitamin D3 (VD3). RUNX2 and VDR unite to cooperatively regulate the expression of numerous genes. In this study, we overexpressed RUNX2 in NIH3T3 fibroblasts concomitantly treated with VD3 and show that RUNX2 alone, or in combination with VD3, failed to promote an osteoblastic phenotype in NIH3T3 cells. However, the expression of numerous osteoblast-related genes was up-regulated by RUNX2 and large-scale gene expression profiling using microarrays identified over 800 transcripts that displayed a twofold or greater change in expression in response to RUNX2 overexpression or VD3 treatment. Functional analysis using gene ontology (GO) revealed GO terms for ossification, cellular motility, biological adhesion, and chromosome organization were enriched in the pool of genes regulated by RUNX2. For the set of genes whose expression was modulated by VD3, the GO terms response to hormone stimulus, chemotaxis, and metalloendopeptidase activity where overrepresented. Our study provides a functional insight into the consequences of RUNX2 overexpression and VD3 treatment in NIH3T3 cells in addition to identifying candidate genes whose expression is controlled by either factor individually or through their functional cooperation. J. Cell. Biochem. 115: 1594–1608, 2014.

KEY WORDS: TRANSCRIPTION FACTOR; TARGET-GENE EXPRESSION; COOPERATIVE REGULATION; OSTEOBLAST; BONE

Skeletal formation is a highly complex developmental process that occurs via two main mechanisms: intramembranous ossification during which mesenchymal condensations are directly converted into mineralizing osteoblasts; and endochondral ossification where a cartilage skeletal anlagen precedes the formation of mineralized bone tissue [Gilbert, 2000]. Studies investigating the molecular mechanisms of skeletal development revealed that the runt-related transcription factor, RUNX2, is critically involved in bone formation. In mice, homozygous null mutations in *Runx2* results in severely disrupted skeletal development that is characterized by the absence of mature osteoblasts and osteoclasts, and leads to defects in both endochondral and intramembranous ossification. Chondrocyte maturation is also perturbed in RUNX2$^{-/-}$ mice as revealed by a reduction in the number of hypertrophic chondrocytes [Komori et al., 1997; Otto et al., 1997]. Consistently, chondrocyte hypertrophy was restored when *Runx2* expression was re-established in RUNX2 null mice [Takeda et al., 2001]. In humans, *Runx2* haploinsufficiency is associated with the skeletal syndrome cleidocranial dysplasia (CCD) that is characterized by several skeletal defects including delayed closure of cranial sutures and hypoplasia/aplasia of clavicles [Mundlos et al., 1997]. RUNX2 coordinates osteoblast differentiation and chondrocyte maturation by regulating the expression of genes such as *Osc*, *Col1a1*, *Spp1*, *Mmp13*, and *Col10a1* [Ducy et al., 1997; Komori, 2010], and exerts control over gene expression by interacting with major signaling networks including vitamin D3 [Paredes et al., 2004; Shen and Christakos, 2005; Komori, 2011].

Activated vitamin D3 (VD3), 1,25-dihydroxyvitamin D3, is a steroid hormone derivative that also plays a pivotal role in bone [Yoshizawa et al., 1997; Haussler et al., 1998]. The actions of VD3 are mediated by the binding of VD3 to the nuclear vitamin D receptor (VDR) that associates with its heterodimeric partner protein, retinoid X receptor (RXR), to regulate target gene expression. VDR regulates bone homeostasis by maintaining calcium and phosphate balance, and achieves this by promoting intestinal absorption of calcium and phosphate, stimulating renal reabsorption of calcium and phosphate,

The authors do not have any conflicts of interest to disclose.
Grant sponsor: National Health and Medical Research Council of Australia.
*Correspondence to: Alexandre S. Stephens, NSW Ministry of Health, Locked Bag 961 North Sydney NSW 2059, Australia. Email: astep@doh.health.nsw.gov.au
Manuscript Received: 16 April 2014; Manuscript Accepted: 21 April 2014
Accepted manuscript online in Wiley Online Library (wileyonlinelibrary.com): 23 April 2014
DOI 10.1002/jcb.24823 • © 2014 Wiley Periodicals, Inc.

and increasing bone resorption facilitating calcium and phosphate release [Haussler et al., 1998; Rojas-Rivera et al., 2010]. Additional direct effects of VD3 signaling in bone have been proposed [Lieben and Carmeliet, 2013] and include a role for VD3 in regulating biomineralization through modulating the levels of pyrophosphate [Lieben et al., 2012]. *GST* pull-down assays showed that VDR could interact with all three RUNX proteins (RUNX1–3) in vitro and suggested that the receptor could potentially modulate their transcriptional activities [Marcellini et al., 2010]. Analysis of evolutionary distinct developing embryos revealed that the co-expression of RUNX2 and VDR has largely become restricted to skeletal elements and is the site where the co-regulation of gene expression by both factors is most likely to occur [Marcellini et al., 2010]. Consistently, RUNX2 and VDR have been shown to cooperatively regulate the expression of bone-related *Osc* [Paredes et al., 2004] and *Spp1* [Shen and Christakos, 2005] genes. More recently, functional cooperation between VDR and RUNX2 was shown to regulate *Osc*, *Rankl,* and *Vdr* mRNA expression [Han et al., 2013].

In this study, we investigated the effects of overexpressing *Runx2* in mesenchymal NIH3T3 fibroblasts. *Runx2*-transduced cells and control (firefly luciferase expressing) cells were assessed for osteogenic phenotypes to determine if RUNX2 was capable of promoting the trans-differentiation of NIH3T3 cells into osteoblast-like cells. Several known stimulators of osteoblast differentiation, including VD3, were also added to the growth medium during cell culture experiments. We show that RUNX2 alone or in combination with stimulators of osteoblastogenesis failed to promote an osteoblast-like phenotype in NIH3T3 cells but enhanced the expression of known osteoblast-related genes. *Runx2*-transduced cells were used as a platform to identify novel gene targets of RUNX2 and VD3 via the application of whole genome microarrays, quantitative PCR and functional analysis based on gene ontology.

MATERIALS AND METHODS

CELL CULTURE AND REAGENTS

NIH3T3 and 293T cells were grown in Dulbecco's Modified Eagle Medium (DMEM, Invitrogen) and MC3T3-E1 cells (subclone 14) were maintained in minimum essential medium (α-MEM, Invitrogen). The culture medium for all cell lines was supplemented to contain 10% fetal bovine serum (FBS, Invitrogen), 1% penicillin/streptomycin solution (Invitrogen), and 1 mM sodium pyruvate (Invitrogen). Supplementation of the culture medium with ascorbic acid to a final concentration of 50 μg/ml and β-glycerophosphate to 10 mM was termed osteogenic medium (OM). For osteoblast differentiation, cells were seeded in 24-well culture plates at a density of 2.5×10^4 cells/well in a total volume of 0.5 ml of medium, and then at 48 h, medium was replaced with OM. Medium was changed every 72 h unless stated otherwise. Dimethyl sulfoxide was purchased from Sigma-Aldrich and used at a final concentration of 1% (v/v). 1α,25-Dihydroxyvitamin D3 (Sigma-Aldrich) was added to the culture medium at a final concentration of 100 nM. Dexamethasone and recombinant BMP2 (Sigma-Aldrich) were used at final concentrations of 4 nm and 300 ng/ml, respectively.

CLONING OF pBABE-RUNX2 AND pBABE-LUX, AND RETROVIRAL PARTICLE PRODUCTION AND INFECTION

pBABE-*Runx2* was constructed by digesting pEF-BOS-*Runx2* [Zhang et al., 2000] with BglII and SalI liberating 1.9 Kbp fragments containing the *Runx2*-I cDNA. The excised fragments were purified and cloned into the BamHI and SalI sites of the retroviral vector pBABE-puro. To serve as a control, the luciferase gene from the pGL3-basic vector (Promega) was excised by digestion with BglII and SalI and cloned into the BamHI and SalI sites of pBABE-puro to create pBABE-lux. Retroviral particles were produced by co-transfection of pBABE retroviral vectors, the VSV-G envelope glycoprotein vector pCSIG, and the Friend murine leukemia virus-based Gag-Pol expression vector pC57GP [Lassaux et al., 2005] in 293T cells using FuGENE HD transfection reagent. Fresh medium was added to cells 24 h post-transfection, and viral supernatants were harvested 48 h later. Viral supernatants were passed through a 0.45-μm pore size filter and used directly for infections. Infections were performed by seeding NIH3T3 cells at 2.5×10^5 cells in 25-cm^2 culture vessels. Twenty four hours later, the medium was replaced with viral supernatant containing 8 μg/ml Polybrene. The cells were incubated with virus for 24 h after which infected cells were selected by replacing the viral supernatant with fresh medium containing 4 μg/ml puromycin. Three separate pooled infected cell lines for each *Runx2* (NIH-RUNX2) and luciferase (NIH-LUX) were expanded in culture prior to use in experiments.

ALKALINE PHOSPHATASE (ALP) ACTIVITY AND DETECTION OF MATRIX MINERALIZATION

The hydrolysis of *p*-nitrophenyl phosphate into *p*-nitrophenol was used to assess the levels of ALP activity. For the assays, cells were washed with 1 volume of PBS and lysed by adding 200 μl of 50 mM Tris-HCl, pH 8.0, and 0.5% Triton X-100 (per well, 24-well plate). 10 μl of cell lysate was incubated with 200 μl of 1 M diethanolamine, 0.5 mM $MgCl_2$, pH 9.8, containing 10 mM *p*-nitrophenyl phosphate for 15–30 min. The reactions were terminated by adding 50 μl of 3 M NaOH and the amounts of *p*-nitrophenol were quantitated by measuring the absorbance at 405 nm. ALP enzyme activity was standardized using purified calf intestinal ALP (New England Biolabs) and normalized to protein content as measured by the DC protein assay kit (Bio-Rad). ALP activity was expressed as nanomoles of *p*-nitrophenyl phosphate converted per min per mg of protein (nanomoles/min/mg protein). Matrix mineralization was assessed using Alizarin Red S staining according to Gregory et al. [Gregory et al., 2004]. Units are absorbance of solubilized Alizarin Red S measured at 405 nm per culture well. One A405 unit represents 2.96 μmol of Alizarin Red S precipitated per culture.

CELLULAR PROLIFERATION ASSAYS

To assess cellular proliferation, growing cells were gently washed with 1 volume of warm PBS and fresh medium containing 3-(4,5-dimethylthiazol-2-yl)-2,5-diphenyltetrazolium bromide to a final concentration of 0.5 mg/ml was added to the wells. After incubating the cells at 37 °C for 3 h, the incorporated dye was solubilized via the addition of 200 μl of isopropyl alcohol containing 0.1% SDS and 0.04 N hydrochloric acid. The levels of solubilized dye were assessed by measuring the absorbance at 570 nm.

RNA EXTRACTION AND cDNA SYNTHESIS

The acid guanidinium thiocyanate/phenol/chloroform method [Chomczynski and Sacchi, 1987] was used to extract RNA from cultured cells. For cDNA synthesis, ~1 μg of RNA was treated with DNase I (Sigma) to remove any contaminating DNA. The RNA was then converted to cDNA using the ImProm-II reverse transcription system (Promega) according to the manufacturer's instructions. Reactions were carried out in 20-μl volumes, and all cDNA samples were diluted 1:5 in DNase-free water prior to qPCR.

PRIMERS AND QUANTITATIVE PCR (qPCR)

The primers used in the study are listed in Table I. Primers were designed from DNA sequences available through the Entrez Nucleotide database and the specificities of candidate primers were assessed by BLAST, BLAT and oligoanalyzer 3.1 analyses. Amplified DNA products were resolved via polyacrylamide gel electrophoresis to verify that the size of amplicons matched the size of products indicated by *in-silico* PCR and that single, specific amplification products were generated. qPCR amplifications were performed in an iCycler iQ Real-Time PCR Detection System (Bio-Rad) using the iQ SYBR green supermix (Bio-Rad). Reactions were carried out in total volumes of 20 μl and included 250 nM of each primer and 2 μl of diluted cDNA template containing 100 ng cDNA. The thermal cycler conditions were as follows: Step 1, 95 °C for 2:30 min; Step 2, 95 °C for 10 s, 59 °C for 10 s and 72 °C for 25 s (45 cycles); step 3, melt curve analysis from 59–95 °C in 0.5 °C increments. The specificities of the PCR amplifications were assessed by the examination of the melt curves to confirm the presence of single gene-specific peaks. The average cycle threshold of *Actb*, *B2m*, *Hmbs*, *Hprt1*, and *Gapdh* internal control genes was used to normalize gene expression data as per the geNorm algorithm [Vandesompele et al., 2002]. Gene expression levels are presented as fold change relative to control NIH-Lux cells.

ILLUMINA MICROARRAY ANALYSIS

Microarray analysis was performed using Illumina MouseWG-6 v2.0 expression beadchips. The microarray samples were prepared by seeding 1.25×10^5 cells per well of six-well culture plates in 5 ml of standard growth medium. After 48 h, the medium was removed and 5 ml of fresh OM, with or without 100 nM VD3, was added to the wells. The cells were cultured for a further 12 days with medium changes taking place every 72 h. After 12 days of culture in OM, the cells were harvested and RNA extracted. 5 μg of RNA from each of the three NIH-Lux and the three NIH-Runx2 cell lines were combined to create pooled RNA samples. The same procedure was followed for cells treated with VD3. The pooled RNA samples (NIH-Lux, NIH-RUNX2, NIH-Lux + VD3, and NIH-RUNX2 + VD3) underwent quality assessment prior to microarray hybridization and scanning. Microarray signal intensities were exported to Microsoft Excel for manipulation and analysis. Two search filters were applied to the microarray gene expression data to identify differentially regulated genes in response to *Runx2* overexpression or VD3 treatment. Firstly, only genes with a microarray signal intensity of 300 or greater were selected (to flag genes that were at least moderately expressed). These genes were then further subset by selecting only those that displayed a greater than twofold change in expression relative to luciferase control. To discover novel gene targets resulting from the cooperative actions of RUNX2 and VD3, the microarray gene expression data was read into R 3.0.1 and a series of rules were applied to the data (as described in the results).

GENE ONTOLOGY (GO) ANALYSIS

The subsets of differentially regulated genes identified through microarray analysis were analyzed to evaluate the significance of GO term overrepresentation and thus provide an insight in the functional consequences of forced RUNX2 expression and VD3 treatment. Enrichment of GO terms was carried out using the DAVID Bioinformatics Resources 6.7 Functional Annotation applet (http://david.abcc.ncifcrf.gov/tools.jsp). Results from the functional annotation charts were exported to Microsoft Excel for analysis. The study samples consisted of all genes from the subsets of differentially regulated transcripts that had an official gene symbol. The background population included all annotated genes from the Illumina MouseWG-6 v2.0 beadchip array. GO terms associated with *P*-values less than 0.01 were flagged as significantly enriched.

STATISTICAL ANALYSIS

For ALP activity and cellular proliferation assays, the significance of mean differences between cell lines and treatment combinations was evaluated using independent samples *t*-tests and analysis of variance with LSD post-hoc tests. qPCR gene expression data were log transformed prior to analysis to improve normality and differences between groups were assessed using analysis of variance with LSD post-hoc tests. Statistical analyses were performed in SPSS

TABLE I. qPCR Gene Expression Primers (5′-3′) Used in the Study

Gene Symbol	Forward primer	Reverse primer
Actb	CTCTGGCTCCTAGCACCATGAAGA	GTAAAACGCAGCTCAGTAACAGTCCG
B2m	CTGCTACGTAACACAGTTCCACCC	CATGATGCTTGATCACATGTCTCG
Gapdh	ACAGTCCATGCCATCACTGCC	GCCTGCTTCACCACCTTCTTG
Hmbs	GAGTCTAGATGGCTCAGATAGCATGC	CCTACAGACCAGTTAGCGCACATC
Hprt1	GAGGAGTCCTGTTGATGTTGCCAG	GGCTGGCCTATAGGCTCATAGTGC
Akp2	ATCATTCCCACGTTTTCACATTCG	AGACATTTTCCCGTTCACCGTC
Dpt	AGATATACACCAGCAGACCCAACAG	CATGGGAAAGGGAGAATTATCCTTC
Mmp13	GTTGGTCATTACTCAAGGCTATGCA	GGCTTGCTGTGTCTTAGCTGGATC
Nfatc1	TCTCAAGGAACGAGAAGGGCT	ATATGCCCTGGTGTGGTCAGA
Osc	GCAGACACCATGAGGACCC	GGTCTGATAGCTCGTCACAAGC
Osx	TGGAATGTACCCCAGTCCTCTCGAC	CCAGGCCTTGCACATATTAAGCATT
Runx2	CAGTCACCTCAGGCATGTC	GCGTGCTGCCATTCGAG

and *P*-values less than 0.05 were used to denote statistical significance. Results are presented as means or mean fold differences, and error bars represent one standard error of the mean.

RESULTS

RUNX2 OVEREXPRESSION USING VIRAL TRANSDUCTION AND PHENOTYPIC EVALUATION OF TRANSDUCED CELLS

The objective of this study was to identify downstream gene targets of two key transcriptional regulators of skeletal development and bone maintenance, RUNX2 and VDR [Ducy et al., 1997; Komori et al., 1997; Yoshizawa et al., 1997; Haussler et al., 1998], and to further explore gene regulatory functions by identifying transcripts cooperatively regulated by RUNX2 and VD3. Viral transduction was used to overexpress human *Runx2*-I cDNA (39-fold, *P*-value < 0.01) in NIH3T3 murine fibroblasts. We hypothesized that the overexpression of RUNX2 in fibroblasts, a cell type derived from the same common progenitor as osteoblasts, would provide a suitable model to examine gene expression changes in response to forced *Runx2* expression.

In order to precisely evaluate the consequences of RUNX2 overexpression at the transcriptome level, we first investigated whether RUNX2 was capable of promoting the trans-differentiation of NIH3T3 fibroblasts. The trans-differentiation capacity of RUNX2 was evaluated by assessing osteoblast phenotypic markers ALP enzyme activity, extracellular matrix (ECM) mineralization, and cellular proliferation (Fig. 1). ALP activity was evaluated at 3, 5, 9, and 12 days post-addition of OM and showed that *Runx2* overexpression did not significantly increase enzyme activity levels at any of the time points (Fig. 1A). Furthermore, the addition of BMP2, a well-known stimulator of ALP enzyme activity, also failed to induce ALP activity levels in luciferase or *Runx2* expressing cells (Fig. 1A). In support of the lack of increased ALP activity in response to *Runx2* overexpression, transduced cells failed to show any signs of ECM mineralization as indicated by the complete absence of Alizarin Red S staining (Fig. 1B). In contrast, MC3T3-E1 pre-osteoblasts induced to differentiate by culturing in OM for the same period of time as the NIH3T3 cell lines produced extensively mineralized ECM (Fig. 1B). A final indicator that RUNX2 overexpression with or without BMP2 supplementation failed to initiate trans-differentiation of NIH3T3 fibroblasts was the inability of the transcription factor to suppress cellular proliferation (Fig. 1C); a requisite step that precedes osteoblast differentiation [Stein et al., 1990].

In a further attempt to determine if *Runx2* overexpression could promote the trans-differentiation of NIH3T3 fibroblasts into osteoblasts-like cells, transduced cells were cultured in OM with a variety of factors (and combinations thereof) that have been demonstrated to stimulate osteoblast differentiation. The cells were harvested 6 days post-addition of OM and assayed for ALP activity. The assay showed that *Runx2* alone or in combination with numerous stimulators of osteoblast differentiation failed to increase ALP activity to levels required to support ECM mineralization as indicated by the vastly lower levels of enzyme activity compared to MC3T3-E1 pre-osteoblasts cultured under equivalent conditions (Fig. 2). The inset of Figure 2 shows that there were some significant changes in ALP activity in response to various treatment

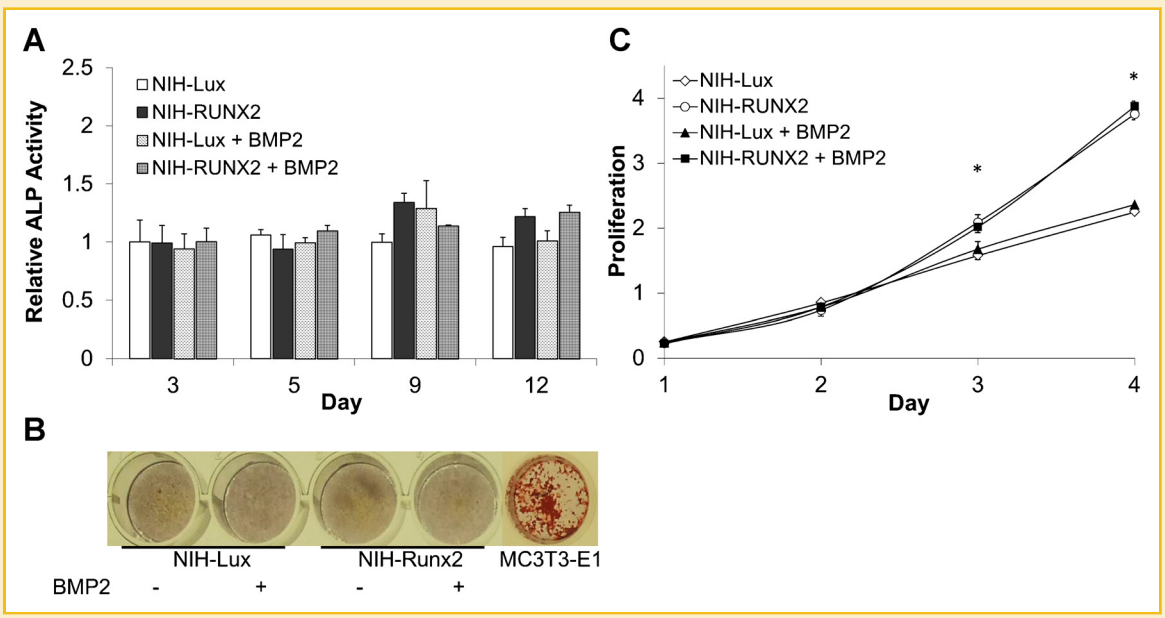

Fig. 1. Alkaline phosphatase activity, extracellular matrix mineralization and cellular proliferation of NIH-Lux and NIH-RUNX2 cells treated with or without recombinant BMP2. (A) Runx2-transduced and luciferase expressing cells were cultured in osteogenic conditions with or without BMP2 and assessed for ALP activity. Results are displayed as fold activity relative to day 3 NIH-Lux cells. (B) NIH-Lux, NIH-RUNX2 and MC3T3-E1 cells were cultured for 12-days in OM and assessed for ECM mineralization using Alizarin Red S staining. (C) Cellular proliferation of NIH-Lux and NIH-RUNX2 cells treated with or without BMP2 assessed using MTT assays after one to four days in culture. * Denotes significantly increased numbers of NIH-RUNX2 cells compared to NIH-Lux cells.

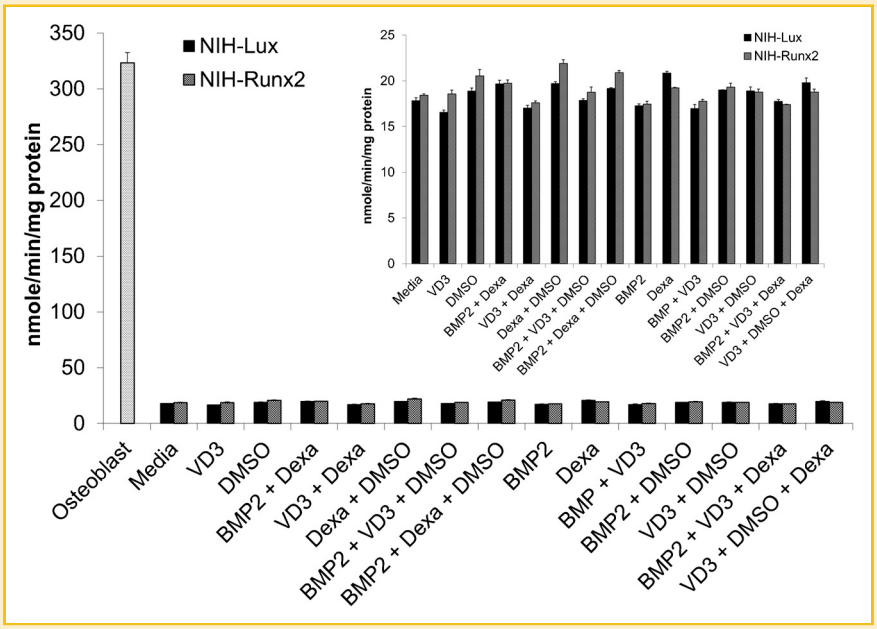

Fig. 2. Alkaline phosphatase activity in NIH-Lux and NIH-RUNX2 cells treated with various combinations of stimulators of osteoblast differentiation. Cell lines were cultured in osteogenic conditions for 6 days prior to the assessment of ALP activity. For comparison, ALP activity in MC3T3-E1 cells, which support ECM mineralization, and were cultured under equivalent conditions, is displayed. VD3, 1,25-dihydroxyvitamin D3; DMSO, dimethyl sulfoxide; Dexa, dexamethasone; BMP2, bone morphogenetic protein 2.

combinations, however the changes were not in any clear or consistent patterns and the levels of enzyme activity reached were of no practical significance.

ILLUMINA WHOLE GENOME MICROARRAY GENE EXPRESSION ANALYSIS AND VALIDATION BY qPCR

Phenotypic investigation of *Runx2*-transduced cells indicated that RUNX2 was not promoting osteoblast trans-differentiation and we believed this would increase the chances of identifying gene targets that were proximal to RUNX2 rather than flagging genes potentially altered as a consequence of a differentiation cascade. To search for downstream gene targets of both RUNX2 and VD3, we implemented quantitative real time RT-PCR (qPCR) and whole genome microarray gene expression analysis. Firstly, the expression of three known RUNX2 target genes was evaluated in transduced cell lines treated with or without VD3 using qPCR (Fig. 3). The analysis showed that RUNX2 was able to significantly increase the expression of *Akp2* (10.4-fold, P-value < 0.01), *Osc* (18.0-fold, P-value < 0.01), and *Osx* (28.4-fold, P-value < 0.01). On the other hand, VD3 did not significantly alter the expression of *Akp2* but reduced the expressions of *Osc* and *Osx* (0.3-fold each; P-values < 0.01). Furthermore, VD3 completely abolished RUNX2 induction of *Akp2* (1.3-fold, P-value $= 0.79$) and also severely blunted RUNX2-induction of *Osx* (2.3-fold, P-value $= 0.03$) suggesting an interaction between the two factors in regulating gene expression. Quantitative gene expression analysis of the three osteoblast-related genes revealed that overexpressed *Runx2* was being translated into active protein that was capable of modulating the activity of target promoters paving the way for subsequent large-scale exploration of changes in gene expression using cDNA microarrays. Microarray analysis revealed 262 genes induced by *Runx2*, 154 genes repressed by *Runx2*, 309 genes induced by VD3 treatment, and 149 genes downregulated by treatment with VD3 (Tables II and III, and Supplementary Tables 1–4). Some notable bone-related genes observed in the pool of differentially regulated transcripts included *Osc*, *Mmp13*, *Ctgf*, and *Flh2*, adding cogency to the approach. To further validate the microarray results, qPCR was carried out on several genes that displayed differential regulation (Fig. 4). Firstly, *Runx2* mRNA levels were quantified in the cell lines and verified that the transcription factor was significantly overexpressed in *Runx2*-transduced cells (38.9-fold and 28.8-fold for *Runx2* and *Runx2* + VD3 cells respectively, P-values < 0.01). The expression of *Dpt*, *Mmp13*, and *Nfatc1* were also examined. *Dpt* was silenced by *Runx2* and VD3 (fold changes of 0.07 and 0.03 respectively, P-values < 0.01), and *Mmp13* was induced by *Runx2* and super-induced by VD3 (21-fold and $>10{,}000$ fold respectively; P-values < 0.01). *Nfatc1* expression was potently decreased by VD3 treatment (0.05-fold, P-value < 0.01) but unaffected by *Runx2* alone (1.5-fold, P-value $= 0.31$). Collectively, the qPCR analyses confirmed the direction and, to a lesser extent, the magnitude of the microarray gene expression results. The more sensitive qPCR analyses suggested that the microarray expression results were likely to have underestimated the true changes in gene expression.

GENE ONTOLOGY ANALYSIS

To describe the biological consequences of *Runx2* overexpression or VD3 treatment in NIH3T3 fibroblasts, functional analysis based on Gene Ontology (GO) was performed. The GO terms that displayed the largest and most significant overrepresentation in the collection of genes that were either induced or repressed by *Runx2* or VD3 were explored (Supplementary Tables 5–8). The numbers of GO terms overrepresented in the pools of differentially regulated genes were

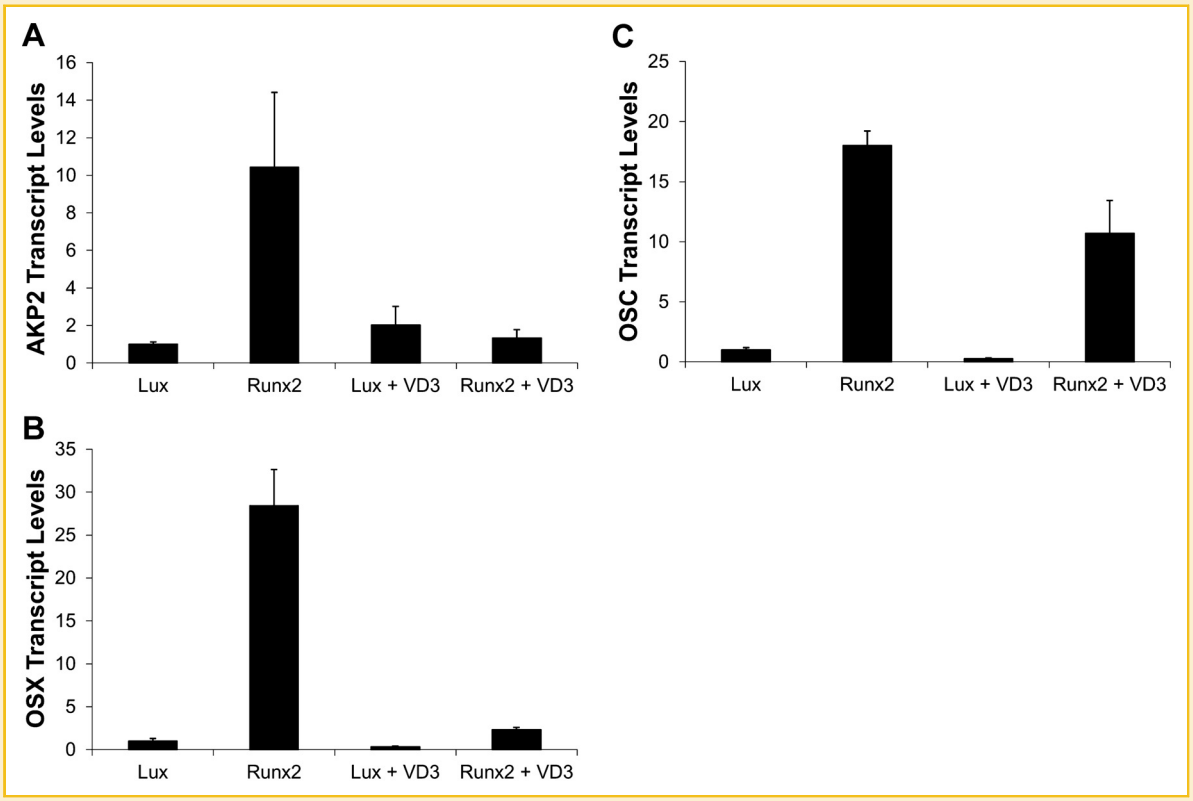

Fig. 3. Quantitative PCR gene expression analysis of Akp2 (A), Osx (B) and Osc (C) in NIH-Lux and NIH-RUNX2 cells treated with or without 100 nM VD3. Data are shown as mean fold change relative to NIH-Lux cells. Three separate pooled stably transfected cell lines for each Lux and RUNX2 were used for the analysis.

16 for *Runx2*-induced, 52 for *Runx2*-repressed, 46 for VD3-induced, and 52 for VD3-repressed. Notable GO classifications enriched in the *Runx2*-induced subset included ossification, consistent with the pivotal role of *Runx2* in bone formation, cellular motility and adhesion, protein-DNA interactions/packaging, and extracellular region. The 52 GO terms enriched in the subset of genes downregulated by *Runx2* could be largely clustered into two groups relating to nucleosome organization and regulation of cell cycle. For the collection of genes whose expression was increased by VD3, the GO terms response to hormone and steroid stimulus in addition to numerous terms relating to morphogenesis and development were overrepresented. Similar to the *Runx2*-repressed set, GO terms enriched in genes downregulated by VD3 could be broadly clustered into classifications for cell cycle regulation and chromatin/nucleosome organization.

GENE REGULATORY INTERACTIONS BETWEEN RUNX2 AND VD3

The joint exposure of cells to *Runx2* and VD3 provided the opportunity to investigate potential cooperative regulatory interactions between the two factors in governing gene expression. To explore this interaction, we analyzed the gene expression profile of *Runx2*-transduced cells that were concomitantly treated with VD3 and applied various rules to the microarray data to capture information on possible regulatory interactions (Table IV). The analysis identified 22 transcripts whose expression was increased only when cells were exposed to both *Runx2* and VD3. In this collection of genes, *Gp49a*, *Osmr*, *Lcn2*, and two RIKEN transcripts displayed the largest fold increases in expression (fold changes ranged from 3.1 to 7.3 relative to luciferase control). For the contrasting design, 18 genes that were unchanged or increased by either *Runx2* or VD3 alone were repressed in the presence of both factors. For this set of genes, *Tmem119*, *Edn1*, *Iigp2*, *Tns1*, and *Ak3l1* displayed the largest fold reductions in gene expression (fold changes ranged from 0.3 to 0.4). Only two genes, *Acpp* (3.7-fold over VD3 and 28.5-fold over *Runx2*) and *Srgap3* (3.8-fold over VD3 and 2.1-fold over *Runx2*), were super-induced by *Runx2* and VD3 displaying synergistic increases in expression while being more modestly increased by each factor independently. For the reverse design, 38 unique genes that were independently repressed by *Runx2* or VD3 displayed a further decrease in expression when both factors were present. For this pool of transcripts, *Birc5*, *Mcm5*, *Pbk*, *Tk1*, *Nusap1*, and *Cdkn3* showed the largest decreases in expression (fold changes ranged from 0.2 to 0.3 relative to *Runx2* and from 0.1 to 0.2 relative to VD3). The final two sets of rules applied to the microarray gene expression data searched for genes that were up-regulated by *Runx2* but then subsequently repressed by the addition of VD3, and genes that displayed elevated expression with VD3 treatment but showed decreased relative expression in *Runx2*-transduced cells treated with VD3. For the first induction–repression set, 26 unique genes showed a pattern of expression that was increased by *Runx2* but then subsequently repressed with the addition of VD3 and for this pool of genes, *Tmem119*, *Cd74*, *Rasl11b*, *Ogn*, and *Itga11* showed the

TABLE II. Genes Displaying Largest Fold Changes in Expression in Response to *Runx2* Over-Expression

Gene name	Symbol	Reference ID	Fold change relative to luciferase control		
			Runx2	VD3	Runx2 + VD3
Runx2 induced					
Kallikrein 1-related peptidase b27	*Klk1b27*	NM_020268.1	27.2	1.4	20.1
Kallikrein 1-related peptidase b21	*Klk1b21*	NM_010642.1	16.6	1.3	12.6
Runt related transcription factor 2	*Runx2*	NM_009820.3	13.4	1.0	7.5
Expressed sequence AU018778	*Au018778*	NM_144930.1	11.5	1.4	3.0
Inhibin beta-A	*Inhba*	NM_008380.1	8.4	0.8	2.1
Serine (or cysteine) peptidase inhibitor, clade G, member 1	*Serping1*	NM_009776.1	7.6	1.0	8.2
CD74 antigen, transcript variant 1	*Cd74*	NM_001042605.1	7.2	1.0	1.5
Aldehyde dehydrogenase family 3, subfamily A1	*Aldh3a1*	NM_007436.1	6.9	0.8	8.5
Vanin 3	*Vnn3*	NM_011979.1	6.6	1.5	22.2
RIKEN cDNA 2610528A11	*2610528a11rik*	XM_987802.1	6.4	0.8	2.4
Kallikrein 1-related pepidase b4	*Klk1b4*	NM_010915.1	6.3	1.1	4.6
Connective tissue growth factor	*Ctgf*	NM_010217.1	6.2	2.7	2.6
cDNA sequence BC064033	*Bc064033*	NM_173375.1	6.2	1.3	1.4
Acyl-Coenzyme A oxidase 2, branched chain	*Acox2*	NM_053115.1	5.9	1.1	2.0
SLIT-ROBO Rho GTPase activating protein 3	*Srgap3*	NM_080448.4	5.6	3.1	11.8
Carboxylesterase 3	*Ces3*	NM_053200.2	5.5	3.1	3.7
ATG9 autophagy related 9 homolog B	*Atg9b*	NM_001002897.3	5.4	1.7	6.6
Fc receptor, IgG, low affinity III	*Fcgr3*	NM_010188.4	5.3	1.1	2.3
Interferon induced transmembrane protein 1	*Ifitm1*	NM_026820.2	5.2	0.4	0.4
Neutrophil cytosolic factor 4	*Ncf4*	NM_008677.1	5.2	0.3	3.4
Runx2 repressed					
Retinoic acid receptor responder (tazarotene induced) 2	*Rarres2*	NM_027852.2	0.0	7.7	0.9
Complement component 4 A (Rodgers blood group)	*C4a*	NM_011413.2	0.1	0.9	0.0
RIKEN cDNA E030010N08 gene	*Loc381284*	XM_355224.1	0.1	0.2	0.1
Radical S-adenosyl methionine domain containing 2	*Rsad2*	NM_021384.3	0.1	1.1	0.1
Small chemokine (C-C motif) ligand 11	*Ccl11*	NM_011330.1	0.1	1.5	0.1
Insulin-like growth factor 2	*Igf2*	NM_010514.2	0.1	1.0	0.1
KN motif and ankyrin repeat domains 1	*Kank1*	NM_181404.5	0.2	1.3	0.2
S100 calcium binding protein A8	*S100a8*	NM_013650.2	0.2	0.8	0.6
Ring finger protein 144A	*Rnf144a*	NM_080563.3	0.2	0.9	0.2
Camello-like 4	*Cml4*	NM_023455.2	0.2	1.6	0.3
Melanocortin 2 receptor	*Mc2r*	NM_008560.2	0.2	0.7	0.2
Phosphodiesterase 6H, cGMP-specific, cone, gamma	*Pde6h*	NM_023898.4	0.2	0.8	0.4
Serum amyloid A 3	*Saa3*	NM_011315.3	0.2	0.7	0.8
Kininogen 1	*Kng1*	NM_023125.2	0.2	0.4	0.5
Dermatopontin	*Dpt*	NM_019759.2	0.2	0.2	0.2
Immunoglobulin superfamily, member 10	*Igsf10*	XM_913941.2	0.2	0.7	0.1
Tissue inhibitor of metalloproteinase 3	*Timp3*	NM_011595.2	0.3	0.4	0.1
GLI-Kruppel family member GLI2	*Gli2*	NM_001081125.1	0.3	0.4	0.2
Metallothionein 2	*Mt2*	NM_008630.2	0.3	0.5	0.4
Cyclin-dependent kinase inhibitor 3	*Cdkn3*	XM_919022.2	0.3	0.4	0.1

greatest repression (fold change ranged from 0.1 to 0.3 relative to *Runx2*). For the opposite design, there were 73 unique genes that displayed heightened expression in response to VD3 treatment but showed decreased relative expression in *Runx2*-transduced cells treated with VD3 suggesting that *Runx2* was preventing VD3 from enhancing the expression of these genes. For this set of genes, *Inmt*, *Prickle1*, *Abcb4*, *Per2*, and *Vdr* showed the greatest reductions ranging in fold changes from 0.1 to 0.2 relative to VD3 treated cells.

DISCUSSION

In this study, we engineered NIH3T3 cells to express high levels of *Runx2* cDNA to determine if the transcription factor could promote the trans-differentiation of the fibroblasts into osteoblast-like cells. Our studies revealed that despite the presence of high levels of gene expression, RUNX2 was not able to increase the activity levels of the osteoblast marker ALP and was insufficient to induce ECM mineralization as indicated by the lack of bone nodule formation. Our results are consistent with previous observations which showed that RUNX2 was incapable of directing the in vitro mineralization of NIH3T3 cells [Byers et al., 2002]. However, the sustained high-level expression of *Runx2* in other cells, namely, MC3T3-E1 preosteoblasts, pluripotent C3H10T1/2 fibroblasts, primary bone marrow stromal cells, primary skeletal myoblasts, and adipose tissue-derived stem cells was shown to facilitate biological mineral deposition [Byers et al., 2002; Byers and Garcia, 2004; Gersbach et al., 2004; Zhang et al., 2006] and suggests that the activation of the

TABLE III. Genes Displaying Largest Fold Changes in Expression in Response to Treatment With VD3

Gene name	Symbol	Reference ID	Fold change relative to luciferase control		
			Runx2	VD3	Runx2 + VD3
VD3 induced					
Matrix metallopeptidase 13	*Mmp13*	NM_008607.1	3.6	189.7	178.7
ATP-binding cassette, sub-family B (MDR/TAP), member 4	*Abcb4*	NM_008830.1	1.4	41.4	6.3
Keratin 17	*Krt17*	NM_010663.2	1.3	33.4	20.8
A disintegrin-like and metallopeptidase	*Adamts1*	NM_009621.3	1.7	15.9	3.1
Acid phosphatase, prostate (Acpp)	*Acpp*	NM_207668.2	2.1	15.8	59.3
Immunoglobulin superfamily containing leucine-rich repeat	*Islr*	NM_012043.2	0.8	15.6	1.1
Indolethylamine N-methyltransferase	*Inmt*	NM_009349.3	1.3	14.2	1.0
Matrix metallopeptidase 3	*Mmp3*	NM_010809.1	0.3	12.8	1.7
Glycerophosphodiester phosphodiesterase domain containing 5	*Gdpd5*	NM_201352.2	1.9	11.8	6.5
UDP-N-acetyl-alpha-D-galactosamine:polypeptide N-acetylgalactosaminyltransferase-like 2	*Galntl2*	NM_030166.1	1.1	11.5	2.3
Purinergic receptor P2Y, G-protein coupled, 14	*P2ry14*	NM_133200.3	1.3	11.1	1.9
Spermine oxidase	*Smox*	NM_145533.1	1.4	10.0	6.7
Vitamin D receptor	*Vdr*	NM_009504.3	1.7	9.8	1.6
PREDICTED: hypothetical protein 9330167E06		XM_988947.1	1.6	8.9	3.0
Transglutaminase 2, C polypeptide	*Tgm2*	NM_009373.3	2.0	8.9	2.5
Prickle like 1	*Prickle1*	NM_001033217.3	1.0	8.1	0.6
Angiopoietin 2	*Angpt2*	NM_007426.3	0.7	8.0	0.4
Retinoic acid receptor responder (tazarotene induced) 2	*Rarres2*	NM_027852.2	0.0	7.7	0.9
	Dm15	scl33011.16_16	1.0	7.0	1.9
Zinc finger protein of the cerebellum 4	*Zic4*	NM_009576.2	2.7	6.9	10.1
VD3 repressed					
Hyaluronan synthase 2	*Has2*	NM_008216.2	0.3	0.0	0.1
Cytochrome P450, family 1, subfamily b, polypeptide 1	*Cyp1b1*	NM_009994.1	0.5	0.1	0.1
RIKEN cDNA E030010N08 gene	*Loc381284*	XM_355224.1	0.1	0.2	0.1
Latent transforming growth factor beta binding protein 1	*Ltbp1*	NM_206958.1	0.6	0.2	0.1
Carbonyl reductase 2	*Cbr2*	NM_007621.1	1.4	0.2	0.7
Secretory leukocyte peptidase inhibitor	*Slpi*	NM_011414.2	0.5	0.2	0.4
Angiotensinogen (serpin peptidase inhibitor, clade A, member 8)	*Agt*	NM_007428.3	0.5	0.2	0.2
Dermatopontin	*Dpt*	NM_019759.2	0.2	0.2	0.2
Lipocalin 2	*Lcn2*	NM_008491.1	0.3	0.2	3.1
Pentraxin related gene	*Ptx3*	NM_008987.3	0.9	0.2	1.0
WAP four-disulfide core domain 12	*Wfdc12*	NM_138684.2	0.5	0.3	0.4
Neutrophil cytosolic factor 4	*Ncf4*	NM_008677.1	5.2	0.3	3.4
Matrix Gla protein	*Mgp*	NM_008597.3	0.7	0.3	0.1
PREDICTED: similar to interferon activated gene 204	*Loc638301*	XM_914287.2	1.8	0.3	0.5
Regulator of calcineurin 2	*Rcan2*	NM_207649.1	0.5	0.3	0.3
Slit homolog 2	*Slit2*	NM_178804.2	0.5	0.3	0.2
RIKEN cDNA B830045N13 gene	*B830045n13rik*	NM_153539.2	0.5	0.3	0.3
Olfactomedin-like 3	*Olfml3*	NM_133859.2	0.9	0.3	0.1
Aquaporin 1	*Aqp1*	NM_007472.2	0.7	0.3	0.7
Interleukin 33	*Il33*	NM_133775.1	0.4	0.3	0.5

osteoblastic mineralization program by RUNX2 involves additional factors that are inherently present in mineralizing cells but not in NIH3T3 cells. We proposed that one such factor could be the potent morphogen BMP2. Autocrine BMP signaling is required to achieve successful in vitro osteoblast differentiation of MC3T3-E1 pre-osteoblasts and mouse bone marrow stromal cells [Xiao et al., 2002]. In addition, the RUNX2-induction of the osteoblastic phenotype is dependent upon an intact BMP signaling apparatus and RUNX2 sensitizes cells to respond to BMP signals [Phimphilai et al., 2006]. However, despite the presence of BMP2, *Runx2* overexpression was still unable to direct ECM mineralization. Furthermore, the culture of *Runx2* overexpressing cells with combinations of numerous known stimulators of osteoblast differentiation [Katagiri et al., 1994; Yamanouchi et al., 1997; Maehata et al., 2006; Stephens et al., 2011] failed to enhance ALP activity to levels that would be required to support mineral deposition indicating that NIH3T3 cells require an additional factor (or factors) to support bone nodule formation.

The next central objective of the study was to identify novel target genes of RUNX2 and the key osteogenic factor VD3, and to gain an insight into the potentially complex gene regulatory interactions of both factors by investigating cooperative regulation of gene expression. The lack of an observed trans-differentiation effect in *Runx2* overexpressing cells suggested that the likelihood of observing global changes in gene expression linked to a differentiation cascade was low. We believe this result was central in permitting the identification of proximal RUNX2 downstream targets by decreasing the chances of identifying changes in gene expression that were the consequence of a large scale and complex global

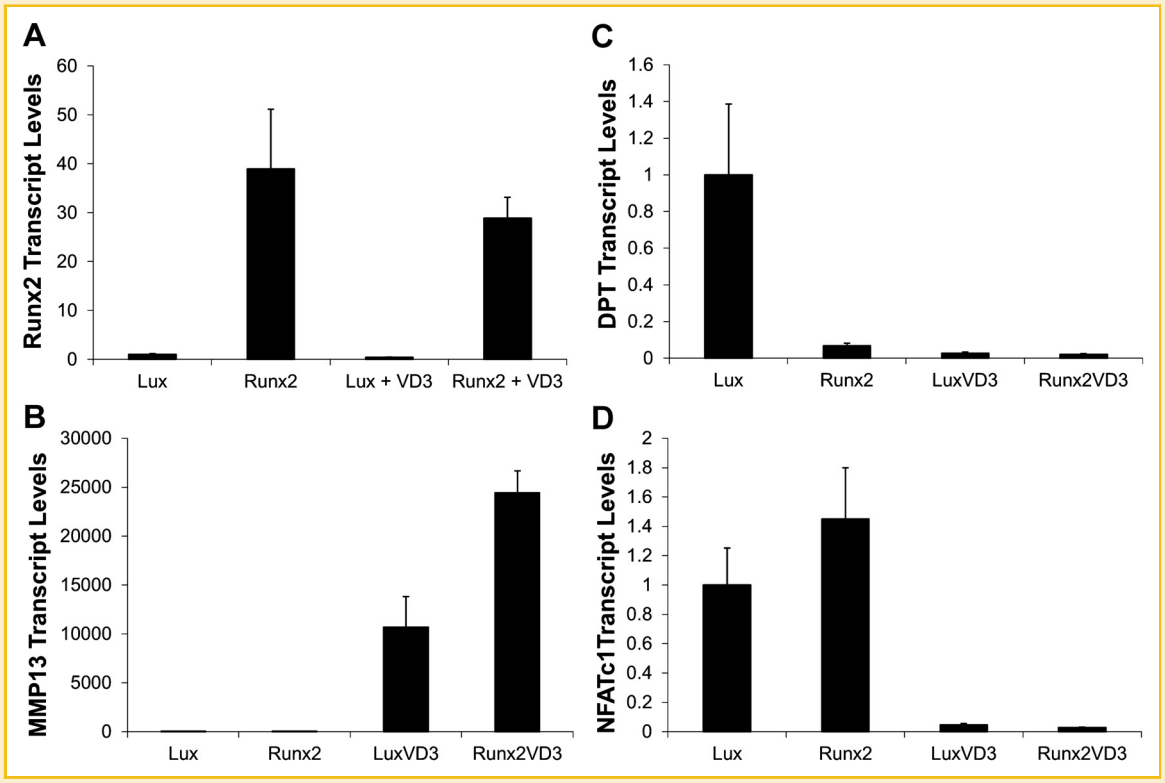

Fig. 4. Validation of microarray gene expression results via quantitative PCR analysis of Runx2 (A), Mmp13 (B), Dpt (C) and Nfatc1 (D) in NIH-Lux and NIH-RUNX2 cells treated with or without 100 nM VD3. Data are shown as mean fold change relative to NIH-Lux cells. Three separate pooled stably transfected cell lines for each Lux and RUNX2 were used for the analysis.

response to cellular (trans) differentiation. qPCR analysis revealed that the osteoblast-related genes *Akp2*, *Osc*, and *Osx* were significantly up-regulated in *Runx2*-transduced cells and indicated that active RUNX2 protein was being produced. Interestingly, the 10-fold induction of *Akp2* by RUNX2 was not accompanied by a corresponding increase in ALP activity indicating a disconnect between transcript levels and protein function. An interaction between RUNX2 and VD3 in controlling gene expression was also revealed by the qPCR analysis that showed that VD3 was able to completely abolish RUNX2-induction of *Akp2* and severely blunt RUNX2 mediated up-regulation of *Osx*. Based on the qPCR evidence indicating active RUNX2 and VD3 signaling, the large-scale search for changes in gene expression was carried out using whole genome microarrays. Over 800 transcripts displayed a twofold or greater change in expression in response to *Runx2* overexpression or treatment with VD3. Notably, several known osteoblast-related genes where observed in the pool of genes that displayed altered expression as a result of forced RUNX2 expression validating our approach to discover novel RUNX2 gene targets. Large changes in gene expression were also observed with VD3 treatment, including that of *Vdr*, whose expression was increased. Quantitative PCR analysis was able to verify the changes in expression of a selected set of genes helping validate the microarray results.

To gain an insight into the biological actions of *Runx2* overexpression and VD3 treatment, functional analysis based on GO was carried out. Consistent with its role as a pivotal regulator of bone formation, the "ossification" GO term was overrepresented in the pool of genes induced by RUNX2. This set of genes included the known RUNX2 gene target *Mmp13* [Jimenez et al., 1999], and the genes *Fhl2* and *Loc100047427* (similar to thyroid hormone receptor). The data also provided evidence to support the involvement of RUNX2 in regulating *Ctgf* expression as previously demonstrated by Ohyama and colleagues [Ohyama et al., 2012]. However, we showed that *Ctgf* expression was increased in response to *Runx2* overexpression whereas Ohyama et al. demonstrated that RUNX2 complexed with SMAD3 negatively regulated TGF-β-induced *Ctgf* expression. The different cellular contexts in which the experiments were performed (murine fibroblasts versus human aortic smooth muscle cells) were likely to explain the different effects observed. Roles for FLH2 and CTGF in bone development and osteoblast differentiation have been previously demonstrated [Luo et al., 2004; Gunther et al., 2005] and our data indicates that RUNX2 could possibly regulate their expression. Other notable GO terms overrepresented in genes up-regulated by RUNX2 included those related to cellular motility and biological adhesion, both of which are critically involved in skeletal patterning and bone development [Lefebvre and Bhattaram, 2010]. Consistently, RUNX2 has recently been shown to occupy the promoters of numerous genes involved in cell adhesion and motility in human osteosarcoma cells [van der Deen et al., 2012]. Cellular motility and biological adhesion genes

TABLE IV. Genes Displaying Differential Expression in Response to Likely Functional Cooperation Between *Runx2* Overexpression and VD3 Treatment

Gene name	Symbol	Reference ID	Fold change relative to luciferase control		
			Runx2	VD3	Runx2 + VD3
Increased by Runx2 and VD3					
	Gp49a	AK089366	1.1	1.1	7.3
	2810439f02rik	AK080904	1.0	1.2	5.2
	F730011o15rik	AK089348	1.3	1.0	4.0
	Osmr	AK087179	1.2	1.1	3.9
Lipocalin 2	*Lcn2*	NM_008491.1	0.3	0.2	3.1
	1700015e05rik	AK005989	1.2	1.0	2.7
PREDICTED: hypothetical protein LOC100038830	*Loc100038830*	XM_001471766.1	1.2	1.1	2.6
Poliovirus receptor	*Pvr*	NM_027514.1	1.3	1.0	2.4
	1810058m03rik	AK007898	1.3	0.8	2.3
Zinc finger, AN1-type domain 2A	*Zfand2a*	NM_133349.2	1.3	1.2	2.3
	3830421f03rik	AK014446	0.6	1.2	2.2
Family with sequence similarity 13	*2610024e20rik*	NM_146084.1	1.3	1.2	2.2
Transmembrane protein 38B	*Tmem38b*	NM_028053.1	1.2	1.0	2.2
Glutathione synthetase	*Gss*	NM_008180.1	1.3	1.3	2.2
RIKEN cDNA 4921505C17	*4921505c17rik*	NM_030168.2	1.1	1.2	2.1
Oncoprotein induced transcript 3	*Oit3*	NM_010959.1	1.0	1.1	2.1
	4833442j19rik	scl0320204.2_97	1.2	1.1	2.1
Fibronectin 1	*Fn1*	NM_010233.1	1.1	1.0	2.0
	2310047k21rik	scl20526.1.1_7	1.3	1.1	2.0
G protein-coupled receptor 137B, pseudogene	*Gpr137b-ps*	NR_003568.1	1.2	0.9	2.0
	1810026b05rik	scl069170.1_207	1.2	1.2	2.0
Interleukin 17 receptor C	*Il17rc*	NM_134159.2	1.2	1.0	2.0
Decreased by Runx2 and VD3					
Transmembrane protein 119	*Tmem119*	NM_146162.1	2.2	1.3	0.3
Endothelin 1	*Edn1*	NM_010104.2	1.7	1.8	0.3
Interferon inducible GTPase 2	*Iigp2*	NM_019440.2	1.1	1.4	0.3
PREDICTED: tensin 1	*Tns1*	XM_984786.1	1.3	1.2	0.4
Adenylate kinase 3-like 1	*Ak3l1*	NM_009647.4	1.2	1.1	0.4
	E130112e08rik	AK053583	1.5	1.1	0.4
Calpain 6	*Capn6*	NM_007603.2	1.4	1.3	0.4
Protein tyrosine phosphatase, receptor type, E	*Ptpre*	NM_011212.2	1.1	1.0	0.4
Zinc finger protein 213	*Zfp213*	NM_001033496.2	1.1	1.1	0.5
Pleiomorphic adenoma gene-like 2	*Plagl2*	NM_018807.5	1.0	1.3	0.5
	3110078m01rik	scl13902.1.1_129	1.2	1.2	0.5
Cyclin D2	*Ccnd2*	NM_009829.3	1.2	1.2	0.5
Ring finger protein 145	*Rnf145*	NM_028862.2	1.0	1.0	0.5
Carboxy-terminal domain, small phosphatase-like	*Ctdspl*	NM_133710.1	1.1	1.2	0.5
Period homolog 2	*Per2*	NM_011066.1	1.1	3.2	0.5
Exocyst complex component 8	*Exoc8*	NM_198103.2	1.0	1.0	0.5
Interferon gamma induced GTPase	*Igtp*	NM_018738.3	1.0	1.2	0.5
Super induced by Runx2 and VD3					
Acid phosphatase, prostate	*Acpp*	NM_207668.2	2.1	15.8	59.3
SLIT-ROBO Rho GTPase activating protein 3	*Srgap3*	NM_080448.4	5.6	3.1	11.8
Super repressed by Runx2 and VD3					
Baculoviral IAP repeat-containing 5	*Birc5*	NM_009689.2	0.3	0.4	0.1
Minichromosome maintenance deficient 5, cell division cycle 46	*Mcm5*	NM_008566.2	0.4	0.4	0.1
PDZ binding kinase	*Pbk*	NM_023209.1	0.5	0.5	0.1
Thymidine kinase 1 (Tk1)	*Tk1*	NM_009387.1	0.4	0.4	0.1
Nucleolar and spindle associated protein 1	*Nusap1*	NM_001042652.1	0.3	0.5	0.1
PREDICTED: cyclin-dependent kinase inhibitor 3, transcript Variant 5	*Cdkn3*	XM_919022.2	0.3	0.4	0.1
Minichromosome maintenance deficient 10	*Mcm10*	NM_027290.1	0.4	0.4	0.1
PREDICTED: antigen identified by monoclonal antibody Ki 67	*Mki67*	XM_001000692.2	0.4	0.5	0.1
Cyclin B1	*Ccnb1*	NM_172301.3	0.3	0.4	0.1
Polo-like kinase 1	*Plk1*	NM_011121.3	0.3	0.4	0.1
PREDICTED: hypothetical LOC640739	*Loc640739*	XM_925296.2	0.4	0.4	0.1

(Continued)

Table IV. (*Continued*)

Gene name	Symbol	Reference ID	Fold change relative to luciferase control		
			Runx2	VD3	Runx2 + VD3
Cell division cycle 20 homolog (S. cerevisiae)	*Cdc20*	NM_023223.1	0.4	0.4	0.1
Cell division cycle associated 2	*Cdca2*	NM_175384.3	0.4	0.4	0.1
Aurora kinase A	*Aurka*	NM_011497.3	0.4	0.4	0.1
Cell division cycle associated 3	*Cdca3*	NM_013538.4	0.3	0.4	0.1
Protein regulator of cytokinesis 1	*Prc1*	NM_145150.1	0.4	0.4	0.1
Histone cluster 1, H2ah	*Hist1h2ah*	NM_175659.1	0.4	0.4	0.1
Tissue inhibitor of metalloproteinase 3	*Timp3*	NM_011595.2	0.3	0.4	0.1
Histone cluster 1, H2ak	*Hist1h2ak*	NM_178183.1	0.4	0.3	0.1
Aurora kinase B	*Aurkb*	NM_011496.1	0.4	0.4	0.1
RIKEN cDNA 3000004C01 gene	*3000004c01rik*	NM_197959.1	0.5	0.5	0.1
Budding uninhibited by benzimidazoles 1 homolog, beta	*Bub1b*	NM_009773.1	0.4	0.4	0.1
Sperm associated antigen 5	*Spag5*	NM_017407.1	0.4	0.4	0.1
Histone cluster 1, H2af	*Hist1h2af*	NM_175661.1	0.4	0.4	0.1
Histone cluster 1, H2ag	*Hist1h2ag*	NM_178186.2	0.4	0.3	0.1
Centromere protein A	*Cenpa*	NM_007681.2	0.4	0.5	0.1
Solute carrier family 38, member 2	*Slc38a2*	NM_175121.3	0.4	0.5	0.1
Kinesin family member 22	*Kif22*	NM_145588.1	0.4	0.4	0.1
Histone cluster 1, H2an	*Hist1h2an*	NM_178184.1	0.4	0.3	0.2
	2010317e24rik	scl072080.6_214	0.3	0.4	0.2
Cell division cycle associated 8	*Cdca8*	NM_026560.3	0.4	0.5	0.2
Kinesin family member 23	*Kif23*	NM_024245.3	0.4	0.4	0.2
Histone cluster 1, H2ai	*Hist1h2ai*	NM_178182.1	0.4	0.4	0.2
RIKEN cDNA 2610510J17 gene	*2610510j17rik*	NM_028131.1	0.4	0.5	0.2
Histone cluster 1, H2ao	*Hist1h2ao*	NM_178185.1	0.5	0.4	0.2
Histone cluster 1, H2ad	*Hist1h2ad*	NM_178188.3	0.5	0.5	0.2
Cell division cycle 2 homolog A (S. pombe)	*Cdc2a*	NM_007659.3	0.5	0.5	0.2
	Brrn1	scl18712.18.1_54	0.5	0.5	0.2
VD3 induced but Runx2 repressed					
ATP-binding cassette, sub-family B (MDR/TAP), member 4	*Abcb4*	NM_008830.1	1.4	41.4	6.3
A disintegrin-like and metallopeptidase (reprolysin type) with Thrombospondin type 1 motif, 1	*Adamts1*	NM_009621.3	1.7	15.9	3.1
Indolethylamine N-methyltransferase	*Inmt*	NM_009349.3	1.3	14.2	1.0
UDP-N-acetyl-alpha-D-galactosamine:polypeptide N-Acetylgalactosaminyltransferase-like 2	*Galntl2*	NM_030166.1	1.1	11.5	2.3
Vitamin D receptor	*Vdr*	NM_009504.3	1.7	9.8	1.6
PREDICTED: hypothetical protein 9330167E06	*9330167e06*	XM_988947.1	1.6	8.9	3.0
Transglutaminase 2, C polypeptide	*Tgm2*	NM_009373.3	2.0	8.9	2.5
Purinergic receptor P2Y, G-protein coupled, 14	*P2ry14*	NM_133200.3	1.4	7.0	1.7
	Dm15	scl33011.16_16	1.0	7.0	1.9
Prickle like 1	*Prickle1*	NM_001033217.3	1.2	6.6	0.9
	Enpp3	AK089553	1.2	6.6	1.7
PREDICTED: similar to RIKEN cDNA 5830484A20 gene	*Loc624083*	XR_035632.1	1.2	5.6	1.2
PREDICTED: gene model 22	*Gm22*	XM_001001798.2	3.0	5.2	1.5
Semaphorin 5A	*Sema5a*	NM_009154.2	1.5	5.0	1.2
Neural precursor cell expressed, developmentally down-Regulated gene 9	*Nedd9*	NM_017464.2	1.6	4.9	1.5
SH3 domain and tetratricopeptide repeats 2	*Sh3tc2*	NM_172628.2	1.4	4.8	1.5
Chemokine (C-C motif) ligand 4	*Ccl4*	NM_013652.2	1.0	4.6	1.2
PREDICTED: tetratricopeptide repeat domain 7B, transcript Variant 1	*Ttc7b*	XM_127105.8	1.9	4.5	1.6
Osteoglycin	*Ogn*	NM_008760.2	4.0	4.1	1.2
RIKEN cDNA 2010011I20 gene	*2010011i20rik*	NM_025912.3	1.2	4.0	1.3
	Samhd1	scl0003030.1_14	1.8	4.0	1.8
	A330060e23rik	AK039553	1.1	3.9	1.2
Growth differentiation factor 5	*Gdf5*	NM_008109.1	1.1	3.7	1.6
Isocitrate dehydrogenase 1 (NADP+), soluble	*Idh1*	NM_010497.2	1.8	3.5	1.6
cDNA sequence BC031353	*Bc031353*	NM_153584.1	1.1	3.4	1.4
Immunoglobulin superfamily containing leucine-rich repeat	*Islr*	NM_012043.2	1.3	3.4	1.0
Regulator of G-protein signaling 16	*Rgs16*	NM_011267.2	1.5	3.3	1.5
Deltex 4 homolog	*Dtx4*	NM_172442.2	1.9	3.3	0.9
SET domain containing 4	*Setd4*	NM_145482.2	1.1	3.2	0.9

(Continued)

Table IV. (*Continued*)

Gene name	Symbol	Reference ID	Fold change relative to luciferase control		
			Runx2	VD3	Runx2 + VD3
Adenosine deaminase, RNA-specific, B1	*Adarb1*	NM_130895.2	1.0	3.1	1.1
Cerebellar degeneration-related protein 2-like	*Cdr2l*	NM_001080929.1	1.2	3.0	1.3
Natriuretic peptide receptor 3	*Npr3*	NM_001039181.1	1.1	3.0	1.1
Thiamine pyrophosphokinase	*Tpk1*	NM_013861.3	1.2	3.0	1.4
	Nrp	AK030358	1.4	2.9	0.9
Angiopoietin 2	*Angpt2*	NM_007426.3	1.0	2.9	1.1
NHS-like 1	*Nhsl1*	NM_173390.3	1.0	2.7	1.0
Transforming growth factor, beta receptor II	*Tgfbr2*	NM_009371.2	1.1	2.7	1.1
Coiled-coil domain containing 28A	*Ccdc28a*	NM_144820.3	1.3	2.7	1.1
	Loc331239	XM_284626.2	1.1	2.6	1.1
Signal peptidase complex subunit 3 homolog	*Spcs3*	NM_029701.1	1.2	2.6	1.3
RGM domain family, member B	*Rgmb*	NM_178615.3	1.1	2.6	1.1
RIKEN cDNA 4932441K18 gene	*4932441k18rik*	NM_178935.2	1.1	2.6	1.3
Gene model 1967	*Gm1967*	NM_001033452.2	1.1	2.5	1.0
Endothelial differentiation, sphingolipid G-protein-coupled receptor, 3	*Edg3*	NM_010101.2	1.0	2.5	1.1
RIKEN cDNA C130026I21 gene	*C130026i21rik*	NM_175219.3	1.2	2.5	1.1
PREDICTED: similar to lysyl oxidase-like 2	*Loc100047339*	XM_001477940.1	1.1	2.5	1.1
Zinc binding alcohol dehydrogenase, domain containing 2	*Zadh2*	NM_146090.4	1.1	2.5	1.1
	Bmf	scl18819.7_87	1.0	2.4	0.6
Tubulin tyrosine ligase-like family, member 5	*Ttll5*	NM_001081423.1	1.0	2.4	1.0
Neutral sphingomyelinase (N-SMase) activation associated factor	*Nsmaf*	NM_010945.1	1.1	2.4	1.0
Myosin VIIa	*Myo7a*	NM_008663.2	1.9	2.3	0.8
Progressive ankylosis	*Ank*	NM_020332.3	1.5	2.3	1.0
Semaphorin 7A	*Sema7a*	NM_011352.2	2.2	2.3	0.7
Complement factor B	*Cfb*	NM_008198.1	1.1	2.3	1.1
RIKEN cDNA 4631426J05 gene	*4631426j05rik*	NM_029935.4	1.5	2.3	1.0
	Plcd1	scl35231.15.1_81	1.7	2.3	1.1
Serine racemase	*Srr*	NM_013761.2	1.0	2.2	0.7
v-Ki-ras2 Kirsten rat sarcoma viral oncogene homolog	*Kras*	NM_021284.4	1.1	2.2	1.0
	Rbpms	AK041118	1.2	2.2	0.7
	Scl0003799.1_2	scl0003799.1_2	1.1	2.2	0.5
	Phxr4	scl37287.1.1_235	1.0	2.2	0.9
Transcription factor 3	*Tcf3*	NM_001079822.1	1.2	2.2	0.6
Transducin-like enhancer of split 1	*Tle1*	NM_011599.3	1.2	2.2	1.0
E26 avian leukemia oncogene 1, 5' domain	*Ets1*	NM_001038642.1	1.5	2.2	0.8
Period homolog 2	*Per2*	NM_011066.1	1.2	2.2	0.6
Procollagen-lysine, 2-oxoglutarate 5-dioxygenase 1	*Plod1*	NM_011122.1	1.1	2.1	0.7
Integrin alpha 1	*Itga1*	NM_001033228.1	1.2	2.1	1.0
Mitotic arrest deficient 1-like 1	*Mad1l1*	NM_010752.3	1.0	2.1	0.9
Methyl-CpG binding domain protein 1	*Mbd1*	NM_013594.1	1.4	2.1	1.0
	4930533k18rik	scl37836.1.334_25	1.1	2.0	0.8
Hypermethylated in cancer 1	*Hic1*	NM_010430.2	1.1	2.0	0.9
SH3 multiple domains 4	*Sh3md4*	NM_172788.2	1.0	2.0	0.9
Runx2 induced but repressed by VD3					
Expressed sequence AU018778	*Au018778*	NM_144930.1	11.5	1.4	3.0
CD74 antigen, transcript variant 1	*Cd74*	NM_001042605.1	7.2	1.0	1.5
Connective tissue growth factor	*Ctgf*	NM_010217.1	6.2	2.7	2.6
cDNA sequence BC064033	*Bc064033*	NM_173375.1	6.2	1.3	1.4
Acyl-Coenzyme A oxidase 2, branched chain	*Acox2*	NM_053115.1	5.9	1.1	2.0
Fc receptor, IgG, low affinity III	*Fcgr3*	NM_010188.4	5.3	1.1	2.3
Solute carrier family 40 (iron-regulated transporter), member 1	*Slc40a1*	NM_016917.2	4.2	1.5	1.3
Osteoglycin	*Ogn*	NM_008760.2	4.0	4.1	1.2
Serine peptidase inhibitor, Kazal type 10	*Spink10*	NM_177829.3	3.3	1.2	1.6
Dihydropyrimidinase-like 3	*Dpysl3*	NM_009468.3	3.3	1.1	1.6
DNA segment, human D4S114	*D0h4s114*	NM_053078.3	3.3	1.7	1.1
Integrin alpha 11	*Itga11*	NM_176922.4	3.0	1.0	0.8
PREDICTED: gene model 22	*Gm22*	XM_001001798.2	3.0	5.2	1.5
Multiple EGF-like-domains 10	*Megf10*	NM_001001979.1	2.8	1.2	1.1
Tribbles homolog 3	*Trib3*	NM_175093.2	2.6	1.2	0.8

(Continued)

Table IV. (*Continued*)

Gene name	Symbol	Reference ID	Fold change relative to luciferase control		
			Runx2	VD3	Runx2 + VD3
RAS-like, family 11, member B	*Rasl11b*	NM_026878.1	2.5	2.0	0.6
Pleckstrin homology domain containing, family G (with RhoGef domain) member 5	*Plekhg5*	NM_001004156.2	2.5	1.1	1.1
Receptor (TNFRSF)-interacting serine-threonine kinase 2	*Ripk2*	NM_138952.3	2.3	1.3	1.1
OTU domain containing 4	*Otud4*	NM_001081164.1	2.2	1.1	0.9
Procollagen, type IV, alpha 6	*Col4a6*	NM_053185.1	2.2	1.7	1.0
Semaphorin 7A	*Sema7a*	NM_011352.2	2.2	2.3	0.7
Transmembrane protein 119	*Tmem119*	NM_146162.1	2.2	1.3	0.3
G protein-coupled receptor 35	*Gpr35*	NM_022320.3	2.2	1.2	0.9
PREDICTED: similar to Bcl2-like protein	*Loc100046608*	XM_001476583.1	2.1	1.4	1.0
PREDICTED: similar to heparan sulfate 6-sulfotransferase 1	*Loc100047260*	XM_001477752.1	2.0	1.3	0.9
	1500005k14rik	scl39926.3_137	2.0	1.2	0.9

that were flagged as being induced by RUNX2 included the integrins *Itga4*, *Itga11*, and *Itgb7*, the protein tyrosine phosphatase *Ptprf*, the microtubule-associated protein *Dclk1*, and the CCN family member *Cyr61*. Significantly, roles for *Dclk1* and *Cyr61* in osteoblast differentiation and function have recently been demonstrated [Su et al., 2010; Zou et al., 2013] and our data suggest that they are likely to be genetically downstream of RUNX2. Consistent with the elevated cellular proliferation observed in *Runx2*-transduced cells, the GO terms enriched in the collection of genes repressed by RUNX2 related to cell cycle regulation, chromosome organization and nuclear division. A suite of genes associated with microtubule function and cytoskeletal organization where also downregulated by RUNX2 and support a role for RUNX2 in controlling cellular division and proliferation. Studies that have investigated the role of RUNX2 in cellular proliferation demonstrated the transcription factor attenuated cellular proliferation [Pratap et al., 2003; Galindo et al., 2005; Teplyuk et al., 2008; Lucero et al., 2013]. However, our data suggests that given the right cellular conditions, RUNX2 can elicit a pro-proliferation effect giving the transcription factor an oncogenic property.

Treatment of NIH3T3 fibroblasts with VD3 lead to vast changes in gene expression and GO terms enriched in the pool of VD3 up-regulated genes included response to hormone stimulus and gland development. Notable genes up-regulated in these two GO terms included *Tgfbr2*, *Tgfb3*, *Jak2*, *Pik3r3*, and *Vdr*, which are all involved in signal transduction. Genes that participate in chemotaxis including the chemokines *Ccl4*, *Ccl9*, *Ccl11*, and *Cxcl10*, and GO terms relating to collagen degradation and metalloendopeptidase activity were also overrepresented. Significantly, VD3 elicited increases in the expression of *Mmp3*, *Mmp10*, *Mmp13*, and *Adamts-2* that all participate in the enzymatic processing of collagen or ECM components [Wang et al., 2003; Nagase et al., 2006]. Similar to RUNX2, GO terms enriched in the subset of genes repressed by VD3 related to nucleosome/DNA packaging, cell cycle control, cytoskeletal organization, cell division, and regulation of cellular proliferation. These GO terms suggest VD3 is likely to have the potential to regulate cell division and proliferation. In the context of bone, the actions of VD3/VDR are in-part mediated through osteoblasts where activated VDR increases the expression of RANKL to promote osteoclast formation [Kim et al., 2006]. VD3 is also hypothesized to inhibit bone mineralization by increasing pyrophosphate (PPi) levels. Bone PPi levels are thought to be increased by the enhanced expression of ENPP1, ENNP3, and ANK, which are involved in the synthesis and transport of PPi [Lieben et al., 2012]. The expression of the genes encoding for these proteins have been shown to be increased by VD3 in osteoblasts [Lieben et al., 2012] and our own microarray data showed that VD3 increased the expression of *Enpp3* (6.6-fold) and *Ank* (2.3-fold). Consistently, qPCR analysis showed that VD3 was able to blunt RUNX2-induction of *Akp2* expression adding further evidence to support a role for VD3 in limiting bio-mineralization. The increased expression of chemokines by VD3 could give rise to local paracrine signals that could serve to recruit osteoclast precursors within the bone microenvironment to promote resorption. Significantly, CCL9 has previously been shown to promote osteoclast differentiation [Okamatsu et al., 2004]. VD3 has also been proposed to promote the remodeling of the local bone environment surrounding osteocytes during times of negative calcium balance [Lieben and Carmeliet, 2013] and the heightened expression of MMPs would be supportive of such an activity.

We next explored changes in gene expression that were likely to have resulted from the interaction between RUNX2 activity and VD3 signaling with the aim to discover potential novel functional cooperation between the two factors. RUNX2 and VDR have been shown to cooperatively regulate the expression of bone-related *Spp1* and *Osc* genes [Paredes et al., 2004; Shen and Christakos, 2005]. Consistently, the overexpression of *Runx2* in VD3-treated rat vascular smooth muscle cells synergistically elevated *Osc* mRNA levels, and also additively increased the expression of *Rankl* and *Vdr* [Han et al., 2013]. Our own qPCR analysis of *Runx2*-transduced NIH3T3 cells showed that RUNX2 and VD3 signals converged to regulate the expression of *Akp2* and *Osx*. Application of search filters to the microarray gene expression data flagged genes that were likely to be co-regulated by RUNX2 and VD3, and ranged from genes that were regulated exclusively in the presence of both factors, genes that displayed additive changes in expression, and transcripts that were induced by one factor but showed relatively decreased expression in cells containing both. The significance of these gene regulatory interactions would need to be further explored by validating the changes in gene expression using qPCR and target-gene promoter transactivation systems while evaluating the

functional relevance of the gene-products within the context of bone or any other applicable biological system. A notable gene that displayed differential regulation in the microarray data was *Vdr*. The analysis showed that *Vdr* was marginally increased by RUNX2 (1.7-fold), highly induced by VD3 (9.8-fold) but only increased 1.6-fold relative to control in *Runx2*-transduced cells treated with VD3 suggesting that RUNX2 prevented VD3-mediated up-regulation of *Vdr*.

While many of the gene expression changes observed in the microarray data were supportive of published studies and relevant in the context of osteoblast and bone biology, only a small proportion were validated by qPCR representing a limitation that is inherently present in large scale gene expression studies. However, we believe most of the microarray derived changes in gene expression were likely to be real given the qPCR data, which agreed well with the microarray results, and the strong concordance observed in RUNX2-mediated changes in gene expression (two-fold change or greater) between duplicate arrays ($r = 0.94$, $n = 357$). A further limitation of microarray platforms is the possibility of ''poor'' probes that contain mismatches or map to problematic genomic regions such as repeat sequences, intergenic areas or intronic loci, and are thus likely to provide unreliable signal [Barbosa-Morais et al., 2010]. Such limitations necessitate that all observed gene expression changes be further investigated to validate the results and evaluate the functional relevance of the changes in expression.

To conclude, we evaluated the effects of over-expressing *Runx2* in mesenchymal NIH3T3 fibroblasts, a cell type derived from the same common progenitor as osteoblasts and chondrocytes. RUNX2 alone or in combination with numerous stimulators/regulators of osteogenic cell differentiation failed to promote an overt osteoblastic phenotype in transduced cells. However, several known RUNX2 gene targets were up-regulated as a consequence of *Runx2* over-expression. Large scale microarray gene expression analysis revealed many genes that displayed differential expression as consequence of *Runx2* overexpression and VD3 treatment, helping identify novel gene targets of both factors as well as flagging genes that are potentially regulated through the functional cooperation of RUNX2 and VD3 signaling.

ACKNOWLEDGMENTS

This work was supported by grants from the National Health and Medical Research Council of Australia (to N. A. M.).

REFERENCES

Barbosa-Morais NL, Dunning MJ, Samarajiwa SA, Darot JF, Ritchie ME, Lynch AG, Tavare S. 2010. A re-annotation pipeline for Illumina BeadArrays: improving the interpretation of gene expression data. Nucleic Acids Res 38:e17.

Byers BA, Garcia AJ. 2004. Exogenous Runx2 expression enhances in vitro osteoblastic differentiation and mineralization in primary bone marrow stromal cells. Tissue Eng 10:1623–1632.

Byers BA, Pavlath GK, Murphy TJ, Karsenty G, Garcia AJ. 2002. Cell-type-dependent up-regulation of in vitro mineralization after overexpression of the osteoblast-specific transcription factor Runx2/Cbfal. J Bone Miner Res 17:1931–1944.

Chomczynski P, Sacchi N. 1987. Single-step method of RNA isolation by acid guanidinium thiocyanate-phenol-chloroform extraction. Anal Biochem 162:156–159.

Ducy P, Zhang R, Geoffroy V, Ridall AL, Karsenty G. 1997. Osf2/Cbfa1: a transcriptional activator of osteoblast differentiation. Cell 89:747–754.

Galindo M, Pratap J, Young DW, Hovhannisyan H, Im HJ, Choi JY, Lian JB, Stein JL, Stein GS, van Wijnen AJ. 2005. The bone-specific expression of Runx2 oscillates during the cell cycle to support a G1-related antiproliferative function in osteoblasts. J Biol Chem 280:20274–20285.

Gersbach CA, Byers BA, Pavlath GK, Guldberg RE, Garcia AJ. 2004. Runx2/Cbfa1-genetically engineered skeletal myoblasts mineralize collagen scaffolds in vitro. Biotechnol Bioeng 88:369–378.

Gilbert SF. 2000. Osteogenesis: The Development of Bones. Developmental Biology. 6th edition. Sunderland, MA: Sinauer Associates pp 474–477. Chapter 14.

Gregory CA, Gunn WG, Peister A, Prockop DJ. 2004. An Alizarin red-based assay of mineralization by adherent cells in culture: comparison with cetylpyridinium chloride extraction. Anal Biochem 329:77–84.

Gunther T, Poli C, Muller JM, Catala-Lehnen P, Schinke T, Yin N, Vomstein S, Amling M, Schule R. 2005. Fhl2 deficiency results in osteopenia due to decreased activity of osteoblasts. EMBO J 24:3049–3056.

Han MS, Che X, Cho GH, Park HR, Lim KE, Park NR, Jin JS, Jung YK, Jeong JH, Lee IK, Kato S, Choi JY. 2013. Functional Cooperation between Vitamin D Receptor and Runx2 in Vitamin D-Induced Vascular Calcification. PLoS One 8:e83584.

Haussler MR, Whitfield GK, Haussler CA, Hsieh JC, Thompson PD, Selznick SH, Dominguez CE, Jurutka PW. 1998. The nuclear vitamin D receptor: biological and molecular regulatory properties revealed. J Bone Miner Res 13:325–349.

Jimenez MJ, Balbin M, Lopez JM, Alvarez J, Komori T, Lopez-Otin C. 1999. Collagenase 3 is a target of Cbfa1, a transcription factor of the runt gene family involved in bone formation. Mol Cell Biol 19:4431–4442.

Katagiri T, Yamaguchi A, Komaki M, Abe E, Takahashi N, Ikeda T, Rosen V, Wozney JM, Fujisawa-Sehara A, Suda T. 1994. Bone morphogenetic protein-2 converts the differentiation pathway of C2C12 myoblasts into the osteoblast lineage. J Cell Biol 127:1755–1766.

Kim S, Yamazaki M, Zella LA, Shevde NK, Pike JW. 2006. Activation of receptor activator of NF-kappaB ligand gene expression by 1,25-dihydroxyvitamin D3 is mediated through multiple long-range enhancers. Mol Cell Biol 26:6469–6486.

Komori T. 2010. Regulation of bone development and extracellular matrix protein genes by RUNX2. Cell Tissue Res 339:189–195.

Komori T. 2011. Signaling networks in RUNX2-dependent bone development. J Cell Biochem 112:750–755.

Komori T, Yagi H, Nomura S, Yamaguchi A, Sasaki K, Deguchi K, Shimizu Y, Bronson RT, Gao YH, Inada M, Sato M, Okamoto R, Kitamura Y, Yoshiki S, Kishimoto T. 1997. Targeted disruption of Cbfa1 results in a complete lack of bone formation owing to maturational arrest of osteoblasts. Cell 89:755–764.

Lassaux A, Sitbon M, Battini JL. 2005. Residues in the murine leukemia virus capsid that differentially govern resistance to mouse Fv1 and human Ref1 restrictions. J Virol 79:6560–6564.

Lefebvre V, Bhattaram P. 2010. Chapter Eight - Vertebrate Skeletogenesis. Organogenesis in Development. Current Topics in Developmental Biology. pp 291–317.

Lieben L, Carmeliet G. 2013. Vitamin D signaling in osteocytes: effects on bone and mineral homeostasis. Bone 54:237–243.

Lieben L, Masuyama R, Torrekens S, Van Looveren R, Schrooten J, Baatsen P, Lafage-Proust MH, Dresselaers T, Feng JQ, Bonewald LF, Meyer MB, Pike JW, Bouillon R, Carmeliet G. 2012. Normocalcemia is maintained in mice under

conditions of calcium malabsorption by vitamin D-induced inhibition of bone mineralization. J Clin Invest 122:1803–1815.

Lucero CM, Vega OA, Osorio MM, Tapia JC, Antonelli M, Stein GS, van Wijnen AJ, Galindo MA. 2013. The cancer-related transcription factor Runx2 modulates cell proliferation in human osteosarcoma cell lines. J Cell Physiol 228:714–723.

Luo Q, Kang Q, Si W, Jiang W, Park JK, Peng Y, Li X, Luu HH, Luo J, Montag AG, Haydon RC, He TC. 2004. Connective tissue growth factor (CTGF) is regulated by Wnt and bone morphogenetic proteins signaling in osteoblast differentiation of mesenchymal stem cells. J Biol Chem 279:55958–55968.

Maehata Y, Takamizawa S, Ozawa S, Kato Y, Sato S, Kubota E, Hata R. 2006. Both direct and collagen-mediated signals are required for active vitamin D3-elicited differentiation of human osteoblastic cells: roles of osterix, an osteoblast-related transcription factor. Matrix Biol 25:47–58.

Marcellini S, Bruna C, Henriquez JP, Albistur M, Reyes AE, Barriga EH, Henriquez B, Montecino M. 2010. Evolution of the interaction between Runx2 and VDR, two transcription factors involved in osteoblastogenesis. BMC Evol Biol 10:78.

Mundlos S, Otto F, Mundlos C, Mulliken JB, Aylsworth AS, Albright S, Lindhout D, Cole WG, Henn W, Knoll JH, Owen MJ, Mertelsmann R, Zabel BU, Olsen BR. 1997. Mutations involving the transcription factor CBFA1 cause cleidocranial dysplasia. Cell 89:773–779.

Nagase H, Visse R, Murphy G. 2006. Structure and function of matrix metalloproteinases and TIMPs. Cardiovasc Res 69:562–573.

Ohyama Y, Tanaka T, Shimizu T, Matsui H, Sato H, Koitabashi N, Doi H, Iso T, Arai M, Kurabayashi M. 2012. Runx2/Smad3 complex negatively regulates TGF-beta-induced connective tissue growth factor gene expression in vascular smooth muscle cells. J Atheroscler Thromb 19:23–35.

Okamatsu Y, Kim D, Battaglino R, Sasaki H, Spate U, Stashenko P. 2004. MIP-1 gamma promotes receptor-activator-of-NF-kappa-B-ligand-induced osteoclast formation and survival. J Immunol 173:2084–2090.

Otto F, Thornell AP, Crompton T, Denzel A, Gilmour KC, Rosewell IR, Stamp GW, Beddington RS, Mundlos S, Olsen BR, Selby PB, Owen MJ. 1997. Cbfa1, a candidate gene for cleidocranial dysplasia syndrome, is essential for osteoblast differentiation and bone development. Cell 89:765–771.

Paredes R, Arriagada G, Cruzat F, Villagra A, Olate J, Zaidi K, van Wijnen A, Lian JB, Stein GS, Stein JL, Montecino M. 2004. Bone-specific transcription factor Runx2 interacts with the 1alpha,25-dihydroxyvitamin D3 receptor to up-regulate rat osteocalcin gene expression in osteoblastic cells. Mol Cell Biol 24:8847–8861.

Phimphilai M, Zhao Z, Boules H, Roca H, Franceschi RT. 2006. BMP signaling is required for RUNX2-dependent induction of the osteoblast phenotype. J Bone Miner Res 21:637–646.

Pratap J, Galindo M, Zaidi SK, Vradii D, Bhat BM, Robinson JA, Choi JY, Komori T, Stein JL, Lian JB, Stein GS, van Wijnen AJ. 2003. Cell growth regulatory role of Runx2 during proliferative expansion of preosteoblasts. Cancer Res 63:5357–5362.

Rojas-Rivera J, De La Piedra C, Ramos A, Ortiz A, Egido J. 2010. The expanding spectrum of biological actions of vitamin D. Nephrol Dial Transplant 25:2850–2865.

Shen Q, Christakos S. 2005. The vitamin D receptor, Runx2, and the Notch signaling pathway cooperate in the transcriptional regulation of osteopontin. J Biol Chem 280:40589–40598.

Stein GS, Lian JB, Owen TA. 1990. Relationship of cell growth to the regulation of tissue-specific gene expression during osteoblast differentiation. FASEB J 4:3111–3123.

Stephens AS, Stephens SR, Hobbs C, Hutmacher DW, Bacic-Welsh D, Woodruff MA, Morrison NA. 2011. Myocyte enhancer factor 2c, an osteoblast transcription factor identified by dimethyl sulfoxide (DMSO)-enhanced mineralization. J Biol Chem 286:30071–30086.

Su JL, Chiou J, Tang CH, Zhao M, Tsai CH, Chen PS, Chang YW, Chien MH, Peng CY, Hsiao M, Kuo ML, Yen ML. 2010. CYR61 regulates BMP-2-dependent osteoblast differentiation through the {alpha}v{beta}3 integrin/integrin-linked kinase/ERK pathway. J Biol Chem 285:31325–31336.

Takeda S, Bonnamy JP, Owen MJ, Ducy P, Karsenty G. 2001. Continuous expression of Cbfa1 in nonhypertrophic chondrocytes uncovers its ability to induce hypertrophic chondrocyte differentiation and partially rescues Cbfa1-deficient mice. Genes Dev 15:467–481.

Teplyuk NM, Galindo M, Teplyuk VI, Pratap J, Young DW, Lapointe D, Javed A, Stein JL, Lian JB, Stein GS, van Wijnen AJ. 2008. Runx2 regulates G protein-coupled signaling pathways to control growth of osteoblast progenitors. J Biol Chem 283:27585–27597.

van der Deen M, Akech J, Lapointe D, Gupta S, Young DW, Montecino MA, Galindo M, Lian JB, Stein JL, Stein GS, van Wijnen AJ. 2012. Genomic promoter occupancy of runt-related transcription factor RUNX2 in Osteosarcoma cells identifies genes involved in cell adhesion and motility. J Biol Chem 287:4503–4517.

Vandesompele J, De Preter K, Pattyn F, Poppe B, Van Roy N, De Paepe A, Speleman F. 2002. Accurate normalization of real-time quantitative RT-PCR data by geometric averaging of multiple internal control genes. Genome Biol 3:RESEARCH0034.

Wang WM, Lee S, Steiglitz BM, Scott IC, Lebares CC, Allen ML, Brenner MC, Takahara K, Greenspan DS. 2003. Transforming growth factor-beta induces secretion of activated ADAMTS-2. A procollagen III N-proteinase. J Biol Chem 278:19549–19557.

Xiao G, Gopalakrishnan R, Jiang D, Reith E, Benson MD, Franceschi RT. 2002. Bone morphogenetic proteins, extracellular matrix, and mitogen-activated protein kinase signaling pathways are required for osteoblast-specific gene expression and differentiation in MC3T3-E1 cells. J Bone Miner Res 17:101–110.

Yamanouchi K, Gotoh Y, Nagayama M. 1997. Dexamethasone enhances differentiation of human osteoblastic cells in vitro. J Bone Miner Metab 15:23–29.

Yoshizawa T, Handa Y, Uematsu Y, Takeda S, Sekine K, Yoshihara Y, Kawakami T, Arioka K, Sato H, Uchiyama Y, Masushige S, Fukamizu A, Matsumoto T, Kato S. 1997. Mice lacking the vitamin D receptor exhibit impaired bone formation, uterine hypoplasia and growth retardation after weaning. Nat Genet 16:391–396.

Zhang X, Yang M, Lin L, Chen P, Ma KT, Zhou CY, Ao YF. 2006. Runx2 overexpression enhances osteoblastic differentiation and mineralization in adipose-derived stem cells in vitro and in vivo. Calcif Tissue Int 79:169–178.

Zhang YW, Yasui N, Ito K, Huang G, Fujii M, Hanai J, Nogami H, Ochi T, Miyazono K, Ito Y. 2000. A RUNX2/PEBP2alpha A/CBFA1 mutation displaying impaired transactivation and Smad interaction in cleidocranial dysplasia. Proc Natl Acad Sci U S A 97:10549–10554.

Zou W, Greenblatt MB, Brady N, Lotinun S, Zhai B, de Rivera H, Singh A, Sun J, Gygi SP, Baron R, Glimcher LH, Jones DC. 2013. The microtubule-associated protein DCAMKL1 regulates osteoblast function via repression of Runx2. J Exp Med 210:1793–1806.

SUPPORTING INFORMATION

Additional supporting information may be found in the online version of this article at the publisher's web-site.